Pol J Aviat Med Bioeng Psychol 2021; 27(3): 5-24
DOI: 10.13174/pjambp.30.08.2024.01

ORIGINAL ARTICLE

# ANATOMY-BASED MODELLING OF THE HUMAN VESTIBULAR RECEPTORS FOR THE PURPOSE OF MOTION CUEING IN DYNAMIC FLIGHT SIMULATORS

Rafał LEWKOWICZ[1], Grzegorz KOWALECZKO[2]

1 Department of Simulator Studies and Aeromedical Training, Military Institute of Aviation Medicine, Warsaw, Poland

2 Faculty of Aviation, Polish Air Force University, Warsaw, Poland

**Source of support:** Own sources

**Author's address:** R. Lewkowicz, Department of Simulator Studies and Aeromedical Training, Military Institute of Aviation Medicine, Krasińskiego 54/56 Street, 01-755 Warsaw, Poland, e-mail: rlewkowicz@wiml.waw.pl

**Introduction:** The motion simulation fidelity depends on the vestibular model used in motion cueing algorithm. Therefore, identifying and selecting the most appropriate mathematical model of the vestibular system is important for motion cueing tasks in motion simulators. This paper presents a method for modelling human vestibular receptors and self-motion sensation.

**Methods:** Previous work in the field of mathematical modeling of vestibular system were summarized and full procedure of modeling the human self-motion sensation was presented. In addition, we tested whether an increased complexity of the model, particularly with regard to the anatomy (position and orientation) of vestibular receptors (semicircular canals and otolith organs), could significantly influence the estimation of human self--motion sensation. To investigate this, the pilot's motion sensation was evaluated during a 20-second real flight in an F-16 aircraft (data from this flight came from an Enhanced Crash Survivable Memory Unit, and is detailed in our previous paper). Simulations were conducted with and without model complexities, specifically regarding the position and orientation of the vestibular receptors, as compared to previous models.

**Results:** It was found that the estimated sensation of angular velocity varies, especially in relation to the pitch angular velocity when the roll velocity is present. The sensed gravito-inertial acceleration also varies, particularly with longitudinal acceleration when the vertical acceleration reaches high values.

**Figures:** 9 • **Tables:** 5 • **References:** 84 • **Full-text PDF:** http://www.pjambp.com •  • **Indexation:** Index Copernicus, Polish Ministry of Science and Higher Education

**Discussion and Conclusions:** The complexity of the model, particularly with regards to the orientation of the vestibular receptors, significantly affects the estimated motion sensation. Nevertheless, further research and verification are required to confirm these findings and evaluate their practical implications in simulators that are equipped with a motion platform.

**Keywords:** mathematical modelling, self-motion sensation, vestibular system, vestibular model

## NOMENCLATURE:

| | |
|---|---|
| CNS | central nervous system |
| SCC | semicircular canal |
| OTO | otolith organ |
| GIA | gravito-inertial acceleration |
| CG | center of gravity |
| $O_E x_E y_E z_E$ | frame of reference fixed to the earth |
| $Hx_H y_H z_H$ | frame of reference fixed to the head |
| $Hx_E y_E z_E$ | head-carried the earth-fixed coordinate system |
| $Nx_{SCC} y_{SCC} z_{SCC}$ | frame of reference fixed to the semicircular canals |
| $Nx_{OTO} y_{OTO} z_{OTO}$ | frame of reference fixed to the otolith organs |
| $\Phi, \Theta, \Psi$ | Euler angles (roll, pitch and yaw, respectively) |
| $a_{xi}, a_{yi}, a_{zi}$ | linear acceleration vector in i-th reference system, along x-, y-, and z-axis, respectively |
| $p_i, q_i, r_i$ | roll, pitch and yaw rate of i-th frame of reference, respectively |
| $\alpha_{SCC}, \alpha_{OTO}$ | afferent neural signals from SCC and OTO, respectively |
| $\Omega_i$ | angular velocity vector of i-th frame of reference |
| $l_h$ | distance between the origins of the head- and the SCC-fixed frames |
| g | acceleration of the earth's gravity |
| $\tau_1$ | long time constant that characterizes the response of the vestibular receptors |
| $\tau_2$ | short time constant that characterizes the response of the vestibular receptors |
| $\tau_L$ | lead time constant that characterizes the response of the vestibular receptors |
| $\tau_A$ | adaptation time constant |

### Subscript

| | |
|---|---|
| *H* | represents coordinate vectors expressed in the head-fixed frame |
| *SCC* | represents coordinate vectors expressed in the SCC-fixed frame |
| *OTO* | represents coordinate vectors expressed in the OTO-fixed frame |

## INTRODUCTION

Daily human activities associated with the motion of the body, as well as by land and sea vehicles, are determined from a sense of the body's position, orientation and motion. umans can maintain their spatial orientation due to their sense of vision, hearing, touch, their vestibular system, and their proprioceptors. The signals from these organs are integrated into the central nervous system (CNS). After the vision system, the second most important source of information for a body's position and motion, on the Earth, is the vestibular system. Receptors in the vestibular system (semicircular canals and otoliths organs) provide the CNS with information about the linear and angular head accelerations [10]. In this way, the CNS can determine the perception of orientation relative to the gravity vector. Knowledge about the vestibular system comes mainly from animal tests, because the small size and location of the vestibular system are main difficulties in its study. For this reason, a number of clinical trials were carried out to investigate the physiological phenomena related to the vestibular system, using the vestibular ocular reflex, or the so-called nystagmus. Direct measurements of the physical quantities within the vestibular system are limited and requires, for example, in vivo measurements [57]. These limitations make theoretical modeling of the vestibular system for an *in vitro* study necessary [53]. Young [80] rightly noted that mathematical models have played an important role in research on the vestibular system over the past century. They range from the torsion pendulum analogies of the semicircular canals (SCC) to the optimal estimator "observer" models for multisensory interactions and adaptation.

Models predicting body motion and the perception of spatial orientation are classic bioengineering problems. Both the laws of classical mechanics and optimal control theory were used to build the model. The first methods for modeling human vestibular system receptors were described in numerous publications [5,20,28,55,68]. Despite these efforts, the development of high fidelity, receptor models are still being undertaken in recent decades [2,35,52,56,65]. An overview and the characteristics of the physical and mathematical models for human vestibular system receptors and the physiological phenomena accompanying their stimulation can be found at work [39].

An appropriate mathematical model of the vestibular organ is particularly important to ensure effective motion cueing in simulators, especially those designed for upset prevention and recovery training [23,27,84] as well as spatial disorientation training [40,42,43,78]. Studies on the pilot's sensation are of interest not only to researchers, but also to aviation accident investigation experts [49,51,64]. Despite this, many of these models have been developed with various simplifying assumptions, to keep the model as simple as possible, with an assumed level of accuracy. A common approach is to assume that the semicircular canals are often aligned with the x-, y- and z-axes of the head-fixed coordinate frame (head-fixed coordinate system defined by Reid's plane [16,31,60] with the origin *H* located at the center of the head). Despite the fact that such simplifications are accepted, it is important to note that for a subject sitting upright in a 2-g force field, the downward deviation of the visually perceived eye level reaches an asymptotic value of approximately 25° [73]. This deviation in the visually perceived eye level is explained by the orientation of the vestibular organ in the skull: the macula utriculi is tilted with the anterior end up at approximately 30° with respect to Reid's baseline [16]. In this case, the subject experienced a change in the pitch angular position – a sensation of backward tilt [73] – often termed the "G-excess illusion" [24]. For pitch tilt perception, the other research [14,61] found that hyper-gravity (i.e., >1 Earth g, as normally experienced) caused a perception of being pitched nose up when the actual pitch angle was <30° forward. Otherwise, when pitched nose down by roughly 30°, the perception was unaffected by hyper-gravity. At this orientation, the approximate plane of the utricular component of the otolith organs was roughly perpendicular to the increased stimulation in hyper-gravity [16,18].

Since the actual geometrical orientation and position of the vestibular system receptors are well known [19,62] this information could have been included both in a one- or two-eared version of the model. Due to the fact that, there are no available papers that describe a complete procedure for anatomy-based physical and mathematical modelling of the human vestibular receptors, a method for modeling these sensors using their anatomical position and orientation was presented in this paper.

## The aim of the study

The aim of this study was (1) to present a complete procedure for modelling a human self-motion sensation based on the physiology of the vestibular system, and (2) to test whether an increased complexity of the model, specifically regarding the anatomy (position and orientation) of vestibular receptors (semicircular canals and otolith organs), could significantly influence the estimation of human self-motion sensation.

We focus only on sensation, as this is the first stage of information processing in the brain (Fig. 1, block highlighted in grey), followed by perception and cognition [15,69]. The points, that we have addressed in this paper include consideration of the self-motion sensation estimated in the head and SCC-fixed reference frames (frames are described in the next section of the paper).

## METHODS

This chapter presents the procedure for modelling the response of the receptors of the vestibular organ and the use of the developed model to estimate the pilot's motion sensation during flight.

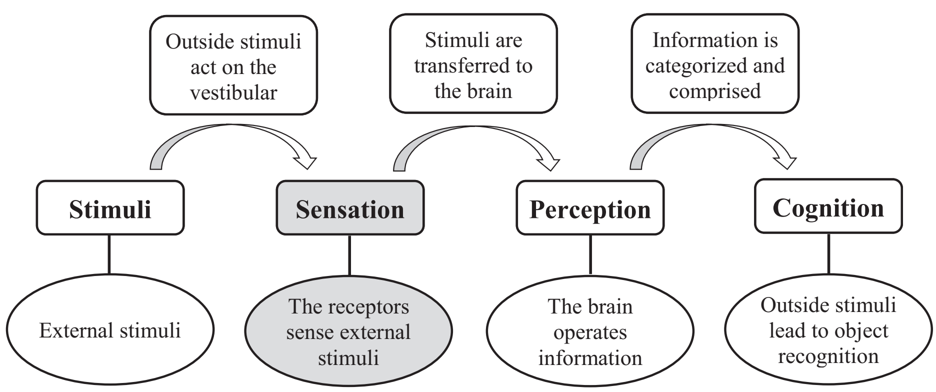


Fig. 1. Stages of information processing in the brain [30].

First, the structure and function of the vestibular organ (anatomy and function) are characterized, especially for its receptors: the semicircular canals and the otolith organ. Physical and mathematical models of these receptors are then presented, using transfer functions for the latter. Finally, the procedure for estimating the pilot's motion sensation is described.

## Vestibular system - anatomy and function

The anatomy and functions of the human vestibular system are well known and have been described in numerous works, i.e. in Hain and Helminski [29] and Silverthorn [63]. The human vestibular system is divided into peripheral and central parts. The peripheral portion consists of semicircular canals (SCC) and the otolith organs (OTO) (Fig. 2), while the central part includes the vestibular nucleus of the brainstem with their connections to other parts of the CNS. Information processing in the brain takes place in three stages [15]: sensation, perception and cognition. The sensation is provided by the receptors (SCC and OTO) that sense the external stimuli (angular and linear motion) and transmit them up to the brain [69]. Therefore, the response of the vestibular organ receptors will be referred to as the sensation of motion.

The labyrinth is an important element in the peripheral part, which closely cooperates with the CNS. It is an organ located in part of the temporal bone on the left and right sides of the human inner ear. The vestibular organ consists of three, connected SCCs, which are sensitive to angular acceleration, while two OTOs (utricle and saccule) are sensitive to linear acceleration.

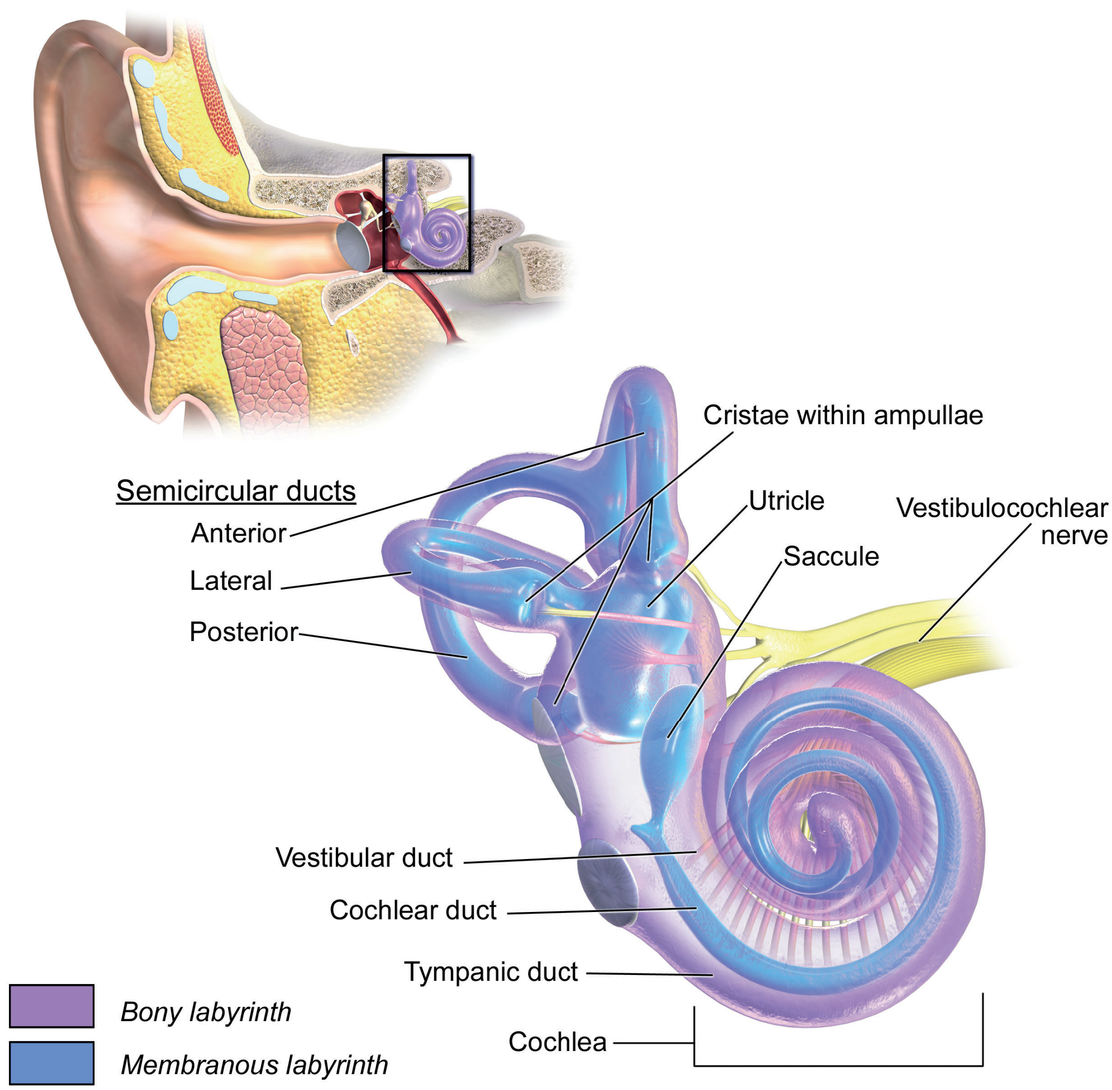


Fig. 2. The vestibular system in the human inner ear [1].

## Semicircular canals

The semicircular canals of the labyrinth bone are formed from three structures filled with perilymph (Fig. 2). Inside them are membranous semicircular ducts containing a liquid called endolymph. The SCCs are located on planes nearly perpendicular to each other and they react to angular accelerations in their respective planes. In place of their connection, an ampulla is formed, where the sensory cells, called the hair cells, are located [63]. The structure of these cells are the same for all five receptors (three SCCs and two OTOs). In the presence of angular acceleration, the inertial flow of endolymph causes deflection of the hair cell sensory cilia in the direction of the fluid motion (counter-acting acceleration).

During SCC motion with constant angular velocity, endolymph achieves the direction of motion and velocity in accordance with the canal displacement. This is a result of endolymph's frictional forces acting on the duct walls, that is, the viscous friction and the cupula elasticity. This phenomenon allows the cupula to return to its normal position. As a result, one has the illusion that the rotational motion has disappeared. Thus, it is assumed that the SCC output signal may be determined by cupula deformation that appears as a result of the canal's angular acceleration [20].

## The otolith organ

The otolith organ consists of two receptors – the utricle and the saccule (Fig. 2). The utricle receptor detects linear acceleration in the horizontal plane, while the saccule does the same in the vertical plane. The otolith organ is located at the base of the SCCs. In each OTO (utricle and saccule), there is a structure known as the macula that is gel coated and covered with calcium carbonate crystals, which are called otoliths or otoconia. There are hair cells immersed in the otolith gel. As a result of the linear acceleration the hair cells deformations of the macula, occur. The direction of these sensory cells in the macula allows for multidirectional polarization. Therefore, it is possible to receive all combinations of translational motions for the head in space.

Reaction of the OTO, which is the linear accelerometer, to inertia acceleration and to gravitational acceleration are similar (Einstein's equivalence principle). Therefore, these receptors can only measure the sum of these accelerations, which can be treated as a vector of resultant gravito-inertial acceleration (GIA):

$$\mathbf{f}_H = \mathbf{g}_{\boldsymbol{H}} - \mathbf{a}_{\boldsymbol{H}} \tag{1}$$

where $g_H$ is gravitational acceleration vector in the head-fixed coordinate system (system description see below), and $a_H$ represents the vector of the head linear acceleration.

According to Einstein's equivalence principle, no set of linear accelerometers alone can distinguish gravitational acceleration $g_H$ (which changes with head orientation during head tilt) from inertial acceleration (which changes with linear acceleration $a_H$ of the head). Therefore, the CNS must use other sensory cues to distinguish tilt from translation. For example, the CNS can use rotational cues provided by the SCCs and vision.

## Physical and mathematical models of the vestibular receptors

### *Semicircular canal models*

**A physical model of the SCC** was based upon data from the study by van Buskirk et al. [5]. It is assumed that the physical model for the SCC has the shape of a torus with the parameters shown in Fig. 3. The narrow part of the canal is defined by the angle *β*, and has a constant circular cross section with radius r. This radius is much smaller than for the major radius of the torus *R*. The utricle is in the area encircled by angle *γ*. The numerical values for the SCC's basic physical and geometric parameters are given in Tab. 1.

**The mathematical model of SCC** dynamics is based on the equation derived by van Egmond et al. [20]:

$$\mathrm{J} \cdot \left( \frac{\mathrm{d}^2 \alpha}{\mathrm{d}t^2} - \frac{\mathrm{d}^2 Q_e}{\mathrm{d}t^2} \right) = \mathrm{C} \cdot \frac{\mathrm{d}Q_e}{\mathrm{d}t} + \mathrm{K} \cdot Q_e(t) \tag{2}$$

and after transformation

$$\ddot{Q}_e(t) + \frac{C}{J} \cdot \dot{Q}_e(t) + \frac{K}{J} \cdot Q_e(t) = \ddot{\alpha}(t)$$

where

| | |
|---|---|
| $\ddot{Q}_e, \dot{Q}_e, Q_e$ | – angular acceleration, velocity, and displacement of the endolymph with respect to the walls of the canal; |
| $\ddot{\alpha}$ | – component of the head's angular acceleration with respect to the spatial axis normal to the plane of the canal; |
| J | – moment of inertia for the endolymph; |
| C | – viscous damping coefficient that occurs during displacement of the endolymph with respect to the walls of the canal; and |
| K | – the coefficient of elasticity associated with cupula movement as a result of fluid displacement in the canal. |

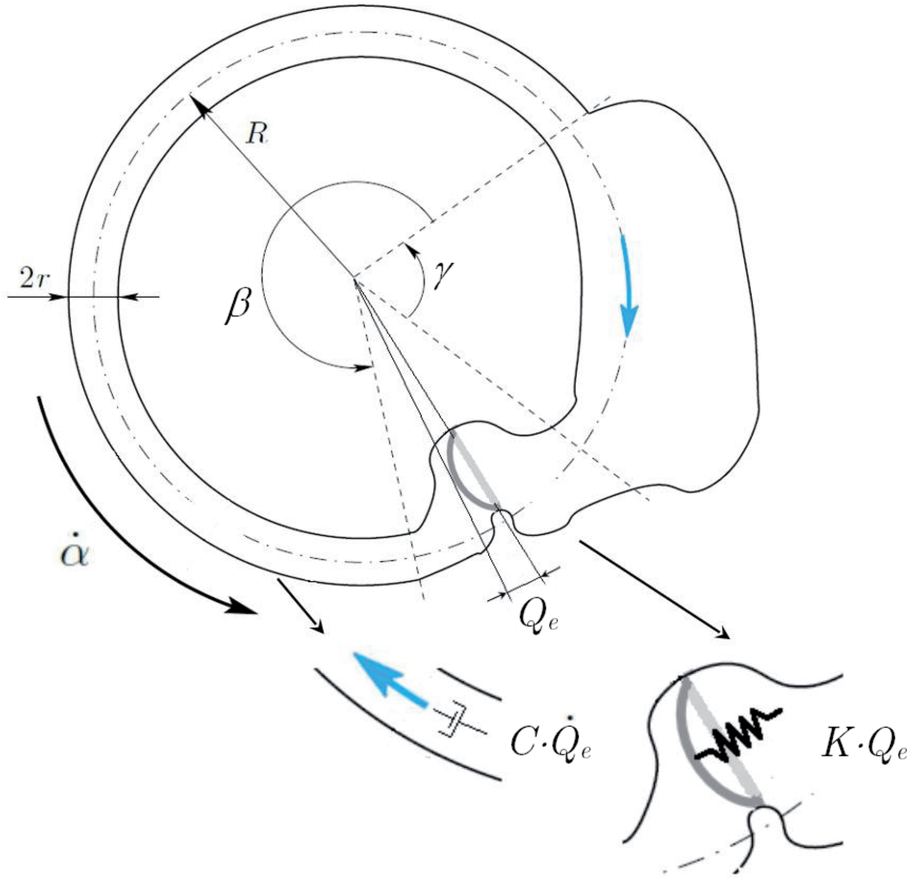


Fig. 3. Physical model for the SCC. The symbols represent: R – radius of the torus; r – canal cross-section radius; $\dot{Q}_e$ ,$Q_e$– angular velocity and displacement of the endolymph with respect to the walls of the canal; $\dot{\alpha}$, α– component of the head's angular velocity and displacement with respect to the spatial axis normal to the plane of the canal; C – viscous damping coefficient that occurs during displacement of the endolymph with respect to the walls of the canal; K – the coefficient of elasticity associated with cupula movement as a result of fluid displacement in the canal.

Due to the small diameter of the canal, which is about 0.3 mm in diameter [17], as described by equation (2), the endolymph's motion is non-oscillating. This means that the characteristic equation of the left side of equation (2) has two real roots [5,47,56,62]:

$$\tau_1^{-1}, \tau_2^{-1} = \frac{C}{2\cdot J}\cdot\left(-1 \pm \sqrt{1-\frac{4\cdot K\cdot J}{C^2}}\right) \tag{3}$$

For the natural motion of the human head, the displacements of endolymph and cupula are directly proportional to the angular velocity $\dot{\alpha}$ of the head rather than to the angular acceleration $\ddot{\alpha}$ [44]. Thus, equation (2) can be written in the form of a Laplace transfer function:

$$\frac{Q_e(s)}{\dot{\alpha}(s)} = \frac{s}{(s+\tau_1^{-1})\cdot(s+\tau_2^{-1})} \tag{4}$$

Further analysis accounts for the extreme eigenvalues of the characteristic equation. If the first term on the left-hand side of equation (2) (representing inertial forces) is small compared to the components of the damping and stiffness forces, then this equation becomes a first-order equation. This gives the root equal to *K/C*. On the other hand, if one considers that, due to the small diameter of the canal (about 0.3 mm), the movement of endolymph in the SCC is strongly suppressed. Therefore, it can be assumed that $4KJ \ll C^2$. This gives the root value equal to *C/J*. Thus, there are two time constants in the modeled system (2) that correspond to non-oscillating movement [56].

$$\tau_1^{-1} \approx \frac{K}{C}, \qquad \tau_2^{-1} \approx \frac{C}{J} \tag{5}$$

The angular displacement of the endolymph $Q_e$ (2) is registered by the nerve receptors. The final signal $\tilde{Q}_e$(s) additionally considers two physiological phenomena accompanying the receptor's stimulation – neural adaptation [54] and the lead

Tab. 1. Physical and geometric parameters for the vestibular system receptors.

| Parameter | Symbol | Value | Source of data (reference) |
|---|---|---|---|
| Radius of the torus | R | $3.2 \times 10^{-3}$ m | [17] |
| Radius of the canal | r | $1.6 \times 10^{-4}$ m | |
| The mean radius of the ampulla | b | $6.8 \times 10^{-4}$ m | |
| Angle circled by the canal | β | 4.4 rad | [5] |
| Angle circled by the utricle | γ | 1.32 rad | |
| Density of the endolymph | $\rho_e$ | 103 kg/m³ | |
| Kinematic viscosity of the endolymph | $\nu_e$ | 10–6 m²/s | [4] |
| Dynamic viscosity of the endolymph | $\mu_e$ | 0.01 g/cm/s | |
| Density of the otoliths | $\rho_{OTO}$ | 2.7x103 kg/m³ | |

Tab. 2. Model parameters for the three SCCs.

| Parameter | Value for the axis rotation | | | Source of data (reference) |
|---|---|---|---|---|
| | $Nx_{SCC}$ | $Ny_{SCC}$ | $Nz_{SCC}$ | |
| $\tau_1$ | 6.1 | 5.3 | 10.2 | [20,45,83] |
| $\tau_2$ | 0.1 | 0.1 | 0.1 | |
| $\tau_A$ | 120 | 120 | 120 | |
| $\tau_L$ | 0.049 | 0.049 | 0.049 | [22] |
| $TH_{SCC}$ [°/s] | 3.0 | 3.6 | 2.6 | [83] |

operator [21]. The first of these phenomena is represented by the transfer function $\tau_A \cdot s(\tau_A \cdot s+1)^{-1}$, and the second has the transfer function equal to $(1+\tau_L \cdot s)$. This transformation is shown below:

dynamics of the torsion pendulum neural adaptation & lead operator

$$\dot{\alpha}(s) \rightarrow \left[\frac{K_{SCC} \cdot s}{(1+\tau_1 \cdot s)\cdot(1+\tau_2 \cdot s)}\right] \rightarrow Q_e(s) \rightarrow \left[\frac{\tau_A \cdot s}{1+\tau_A \cdot s}\right] \cdot [1+\tau_L \cdot s] \rightarrow \tilde{Q}_e(s)$$

Finally, the transfer function for any of the three SCCs is equal to:

$$\frac{\tilde{Q}_e(s)}{\dot{\alpha}(s)} = \frac{K_{SCC} \cdot s}{(1+\tau_1 \cdot s)\cdot(1+\tau_2 \cdot s)} \cdot \frac{\tau_A \cdot s}{1+\tau_A \cdot s} \cdot (1+\tau_L \cdot s) \tag{6}$$

where :

| | |
|---|---|
| $\tilde{Q}_e(s)$ | – long time constant, which defines the slow cupula movement returning to its original position after deformation; |
| $\ddot{\alpha}$ | – the "sensed" angular displacement of endolymph that accounts for neural adaptation and the lead components; – angular velocity of the head; |
| $\tau_1 \approx C \cdot K^{(-1)}$ | – the "sensed" angular displacement of endolymph that accounts for neural adaptation and the lead components; – angular velocity of the head; |
| $\tau_2 \approx J \cdot C^{(-1)}$ | – short time constant, which describes the fast movement of fluid in the canal; |
| $K_{SCC}=\tau_2 \cdot \tau_2$ | – a coefficient characterizing the sensitivity of the endolymph to the displacement, which is the result of angular acceleration [impulses per second/(°/s2)]; |
| $\tau_A$ | – adaptation time constant; and |
| $\tau_L$ | – time constant for the lead operator. |

Additionally, in the SCC dynamics model (6), the sensitivity threshold for $TH_{SCC}$ must be considered. Its values are presented in the Tab. 2 along with other parameters describing the SCC dynamics.

## Otolith organ model

**The physical model of the OTO** is shown in Fig. 4. Both hair cells are embedded into an otolith gel layer and otolith stones-layer model are considered. The last upper layer consists of endolymph. This liquid has a lower density than the density of an otolith.

According to the d'Alembert' principle, is assumed that the sum of all external and inertia forces acting on the otolith organ is equal to zero:

$$F_b + F_c + F_k + F_w - Q_x = 0 \tag{7}$$

Substituting into (7) the formulas for individual forces (enclosed in the Fig. 4 caption), the otolith's motion can be described as follows:

$$m_{OTO}\ddot{x}_{OTO} + c\dot{x} + kx = m_{OTO}g_x - (g_x - \ddot{x}_E)\rho_e V_{OTO} \tag{8}$$

After account for $V_{OTO} = V_e = m_e/p_e$, $x_{OTO}=x+x_E$ and dividing both sides by $m_{OTO}$ yields:

$$\ddot{x} + \ddot{x}_E + \frac{c}{m_{OTO}}\dot{x} + \frac{k}{m_{OTO}}x = g_x - (g_x - \ddot{x}_E)\frac{m_e}{m_{OTO}} \tag{9}$$

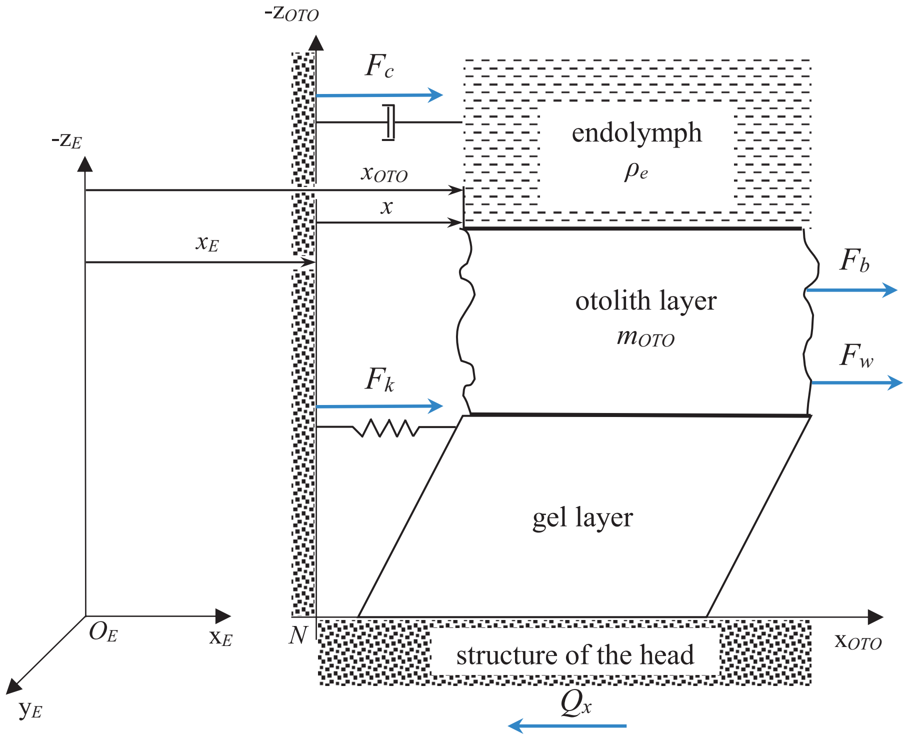


Fig. 4. Physical model of the OTO. The symbols represent: x – otolith displacement with respect to the head; $x_E$ – absolute displacement of the head; $x_{OTO}$ – absolute displacement of the otoliths ($x_{OTO} = x+x_E$); $m_{OTO}$ – mass of the otoliths; $\rho_{OTO}$ – density of the otoliths; $\rho_e$ – density of the endolymph; $F_b=m_{OTO}d^2x_{OTO}/dt^2$– inertial force; $F_k=kdx/dt$ – elastic force; $F_c=cdx/dt$– damping force; $Q_x=m_{OTO}g_x$– weight of the otoliths, where $g_x$ is a component of the gravity acceleration vector acting along the $Nx_{OTO}$-axis; $F_w$– displacement force ($F_w=(g_x- d^2x_E/dt^2)\rho_eV_{OTO}$), where $d^2x_E/dt^2$ is the head's linear acceleration with respect to the Earth-fixed, inertial reference system, while $V_{OTO}=m_{OTO}/\rho_{OTO}$ is the otolith's volume, which is equal to the volume of the displaced endolymph $V_e=V_{OTO}$.

Finally, after the transformation we have the following equation:

$$\ddot{x} + \frac{c}{m_{OTO}}\dot{x} + \frac{k}{m_{OTO}}x = \left(1 - \frac{\rho_e}{\rho_{OTO}}\right)(g_x - \ddot{x}_E) \quad (10)$$

Equation (10) describes the otolith's displacement x under the influence of gravitational acceleration g and the linear acceleration of the head, which interact in the plane parallel to the otolith's layer. Considering that $f_x=(g_x-d^2x_E/dt^2)$ is the GIA, **the mathematical model for the OTO dynamics** can be expressed as follows [25]:

$$\ddot{x}(t) + \frac{c}{m_{OTO}} \cdot \dot{x}(t) + \frac{k}{m_{OTO}} \cdot x(t) = f(t) \cdot \rho_{OTO/e} \quad (11)$$

where:

| | |
|---|---|
| x(t) | – displacement of the otolith's layer with respect to the head; – the otolith's mass; |
| $m_{OTO}$ | – the otolith's mass |
| c, k | – respective viscous damping and elasticity coefficients for the gel layer; |
| f(t) | – GIA component acting in the plane parallel to the otolith's layer; |
| $\rho_{OTO/e}$ | – coefficient, which takes into account the densities of the otoliths and endolymph layers [26]: |

$$\rho_{OTO/e} = 1 - \frac{\rho_e}{\rho_{OTO}} \quad (12)$$

where $\rho_e$ – density of the endolymph, and $\rho_{OTO}$ – density of the otolith layer.

Using similar calculations and transformations, as applied to the SSC model (6), the transfer function, with two characteristic time constants [82], for the OTO model is determined.

$$\frac{\tilde{x}(s)}{f(s)} = K_{OTO} \cdot \frac{1 + \tau_{L\,OTO} \cdot s}{(1 + \tau_{1OTO} \cdot s)\ \ (1 + \tau_{2OTO} \cdot s)} \quad (13)$$

| | |
|---|---|
| $\tilde{x}(s)$ | – the "perceptible" displacement of the otolith layer and accounting for the lead operator ($1+\tau_{LOTO}s$); |
| $\tau_{1OTO}$ | – long time constant that characterizes the damping properties of the gel layer; |
| $\tau_{2OTO}$ | – short time constant that characterizes the elasticity properties of the gel layer; |
| $\tau_{LOTO}$ | – lead time constant for the OTO; |
| $K_{OTO}$ | – a coefficient described as follows: |

$$K_{OTO} = \rho_{OTO/e} \cdot \tau_{1OTO} \cdot \tau_{2OTO} \quad (14)$$

Three identical models for the OTO (13) have been used to describe the full model for the dynamics of the OTO (utricle and saccule): one for each axis of the OTO-fixed coordinate system. Moreover, the model account for the threshold of perception $TH_{OTO}$. Its values and the values of other parameters for the OTO are presented in Tab. 3.

### *The human vestibular system model*

The vestibular system model includes three SCCs (6) and two OTOs (13) that account for their anatomical location and the actual geometrical orientation [19]. Only one model, located at the center of the head, is used to represent both vestibular organs. Moreover, it is assumed that the SCCs are insensitive to linear acceleration and that the modeled vestibular system receptors have linear response characteristics.

The OTOs were modelled using a diagonal transfer function matrix. This matrix represents the three-dimensional responses of the two otolith organ receptors (utricle and saccule). The geometry of the three SCCs was modelled with the relationship derived later in the article.

The phenomena of habituation (increase in the receptor threshold stimulation for repeated types of stimulus) and restitution (the process of decay stimulation) have been omitted because they relate to CNS processing. In the simplified model of the vestibular system used to compare the response with that of the system with the actual geometrical location and orientation, we included the canals and otoliths as aligned with the x-, y- and z-axes of the head.

### *Coordinate systems and their transformation*

The following right-handed coordinate systems are applied to determine the linear acceleration and the angular velocity acting on the vestibular system sensors (Fig. 5):

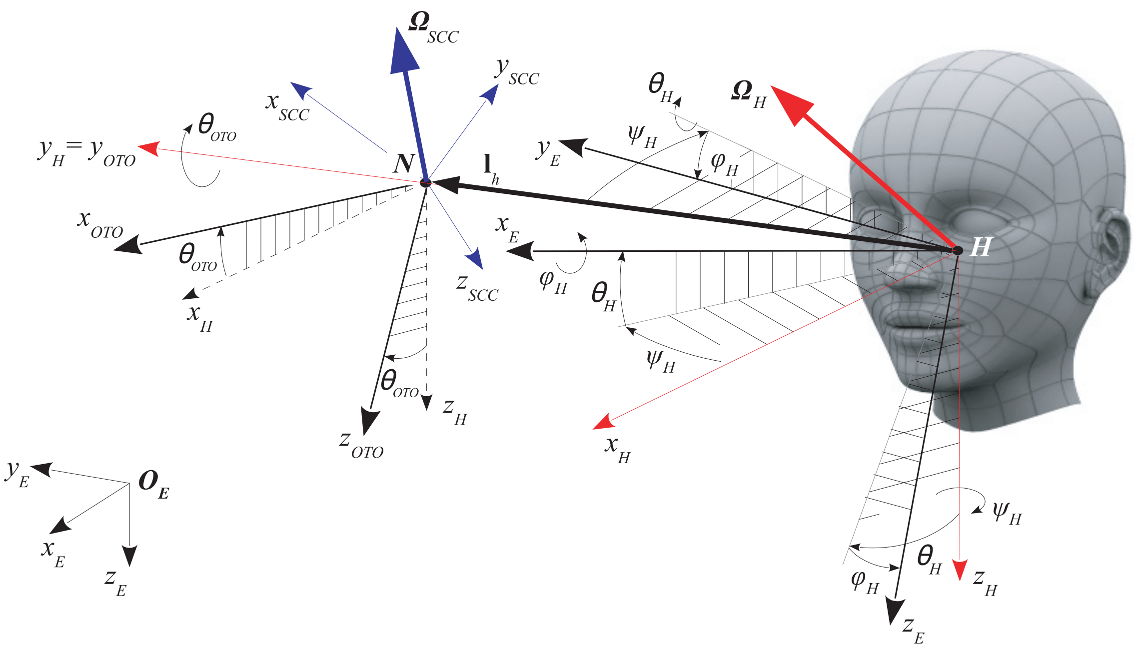

Fig. 5. Coordinate reference systems.

Tab. 3. Parameters of otolith organ model (utricle and saccule).

| Parameter | Value for the axis | | | Source of data (reference) |
|---|---|---|---|---|
| | $Nx_{OTO}$ | $Ny_{OTO}$ | $Nz_{OTO}$ | |
| $\tau_{1OTO}$ | 0.5 | 0.5 | 0.5 | [34] |
| $\tau_{2OTO}$ | 0.016 | 0.016 | 0.016 | |
| $\tau_{AOTO}$ | 1 | 1 | 1 | |
| $K_{OTO}$ | 3.4 | 3.4 | 3.4 | |
| $TH_{OTO}$ [m/s²] | 0.17 | 0.17 | 0.28 | [83] |

- $Hx_Hy_Hz_H$ – a rectangular, head-fixed coordinate system defined by Reid's plane [16,31,60] with the origin H located at the center of the head;
- $Hx_Ey_Ez_E$ – a moving rectangular, head-fixed coordinate system parallel to an Earth-fixed inertial reference system with the origin H located at the center of the head;
- $Nx_{scc}y_{scc}z_{scc}$ – a non-rectangular, SCC-fixed coordinate system with the origin N located at the point of intersection for the axis defined by the normal vectors to the planes of the superior, horizontal, and posterior SCC anatomical positions (Fig. 6);
- $Nx_{OTO}y_{OTO}z_{OTO}$ – a rectangular, OTO-fixed coordinate system with the origin located at the same point N as for the system. Its axes are defined by the anatomical positions of the utricle and saccule planes.

For the transformation coordinates between these systems, Z→Y→X rotation sequences have been applied. An elementary angle of rotation defines the relative position of two coordinate systems:

a) for transformation from the $Hx_E\,y_E\,z_E$ to the $Hx_H\,y_H\,z_H$ system, the following Euler angles (Fig. 5) are used: $\psi_H$, $\theta_H$, $\Phi_H$. Transformation matrix $L_{H/E}$ has the form:

$$L_{H/E} = \begin{bmatrix} c\theta_H \cdot c\psi_H & c\theta_H \cdot s\psi_H & -s\theta_H \\ s\phi_H \cdot s\theta_H \cdot c\psi_H - c\phi_H \cdot s\psi_H & s\phi_H \cdot s\theta_H \cdot s\psi_H + c\phi_H \cdot c\psi_H & s\phi_H \cdot c\theta_H \\ c\phi_H \cdot s\theta_H \cdot c\psi_H + s\phi_H \cdot s\psi_H & c\phi_H \cdot s\theta_H \cdot s\psi_H - s\phi_H \cdot c\psi_H & c\phi_H \cdot c\theta_H \end{bmatrix} \quad (15)$$

where c = cos, s = sin

where

$\Theta_H$ – pitch angle between the $Hx_E$-axis and the local horizontal plane $Hx_Hy_H$;

$\Psi_H$ – yaw angle between the $Hx_E$-axis projection on the horizontal plane $Hx_Hy_H$ and the $Hx_H$-axis;

$\Phi_H$ – roll angle between the $Hy_E$-axis and the horizontal plane $Hx_Hy_H$.

b) for transformation from the $Hx_H\,y_H\,z_H$ system to the $Nx_{SCC}\,y_{SCC}\,z_{SCC}$ system, the following angles (Fig. 6) are used:
   - to alight the $Hx_H$-axis with the $Nx_{SCC}$-axis – yaw angle $\Psi_s$ about the $Hz_H$-axis, and pitch angle $\Theta_s$ about the $Hy'_H$ -axis;
   - to alight the $Hy_H$-axis with the $Ny_{SCC}$-axis – yaw angle $\Psi_p$ about the $Hz_H$-axis, and roll angle $\Phi_p$ about the $Hx'_H$ – axis; and
   - to alight the $Hz_H$-axis with the $Nz_{SCC}$-axis - pitch angle $\Theta_h$ about the $Hy_H$-axis, and roll angle $\Phi_h$ about the $Hx'_H$-axis.

Performing the rotation presented in Fig. 7 has been determined for the transformation matrix $L_{SCC/H}$ [50]:

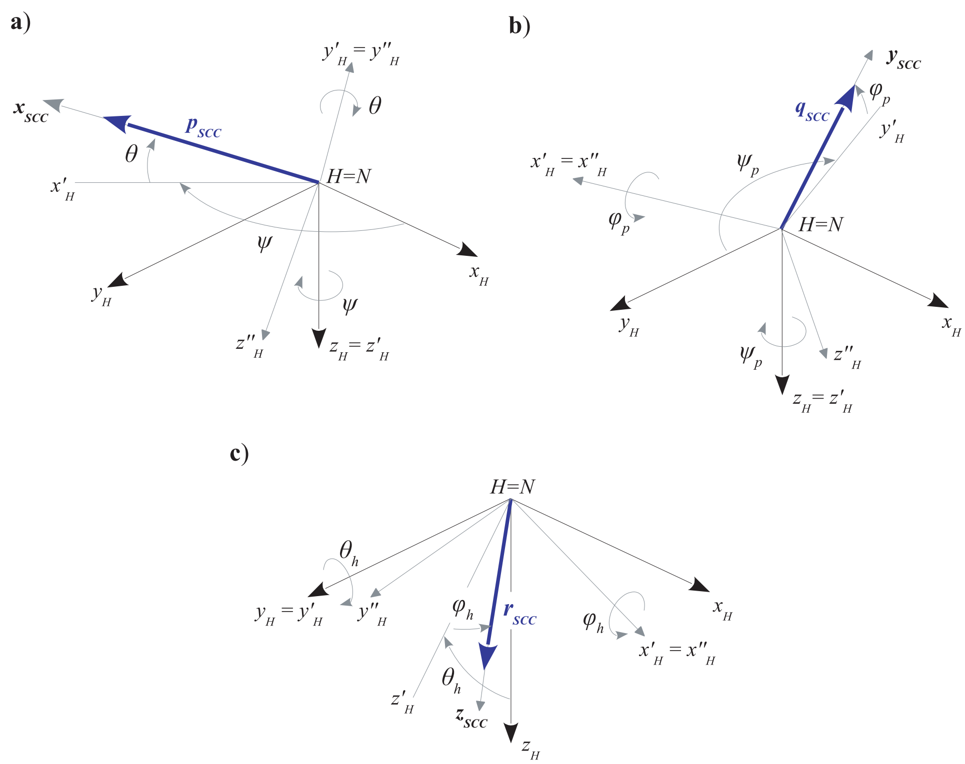


Fig. 6. Mutual position of the coordinate systems $Hx_Hy_Hz_H$ and $Nx_{SCC}y_{SCC}z_{SCC}$ for a) superior, b) posterior, and c) horizontal semicircular canal.

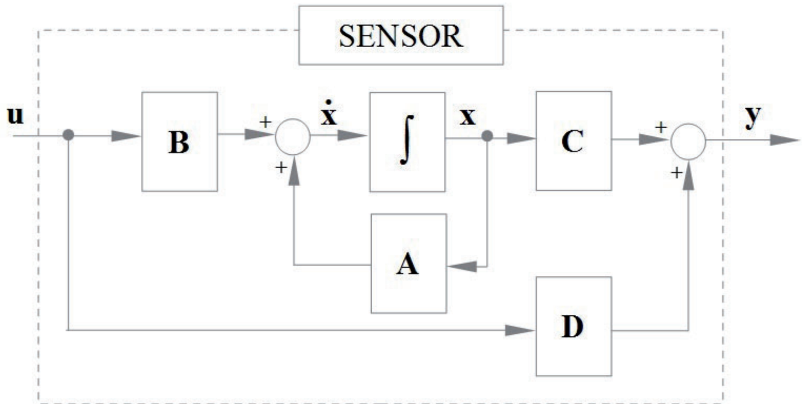


Fig. 7. Block diagram of signal processing by the vestibular system sensor (receptor).

$$\mathbf{L}_{SCC/H} = \begin{bmatrix} \cos\psi_s \cdot \cos\theta_s & \sin\psi_s \cdot \cos\theta_s & -\sin\theta_s \\ -\sin\psi_p \cdot \cos\phi_p & \cos\psi_p \cdot \cos\phi_p & \sin\phi_p \\ \sin\theta_h \cdot \cos\phi_h & -\sin\phi_h & \cos\theta_h \cdot \cos\phi_h \end{bmatrix} \quad (16)$$

The values of the above-mentioned angles are given in Tab. 4.

Tab. 4. Euler angles in radians, which define orientations for the versors perpendicular to the SCC's planes relative to the $Hx_Hy_Hz_H$ system [62].

| | | | |
|---|---|---|---|
| $\hat{e}_{SCCx}$ | $\psi_s \approx 2.212$ | $\theta_s \approx 0.177$ | $\phi_s = 0$ |
| $\hat{e}_{SCCy}$ | $\psi_p \approx 2.336$ | $\theta_p = 0$ | $\phi_p \approx -0.274$ |
| $\hat{e}_{SCCz}$ | $\psi_h = 0$ | $\theta_h \approx -0.331$ | $\phi_h \approx 0.038$ |

c) transformation from the $Hx_Hy_Hz_H$ system to the $Nx_{OTO}y_{OTO}z_{OTO}$ system is obtained using the rotation angle $\theta_{OTO}$ (Fig. 5), between the $Nx_{OTO}$-axis and the horizontal plane $Hx_Hy_H$.

Transformation matrix $L_{OTO/H}$ has the form:

$$\mathbf{L}_{OTO/H} = \begin{bmatrix} \cos\theta_{OTO} & 0 & -\sin\theta_{OTO} \\ 0 & 1 & 0 \\ \sin\theta_{OTO} & 0 & \cos\theta_{OTO} \end{bmatrix} \quad (17)$$

The following real environmental stimuli act upon the human body (relative to the head): angular velocity $\Omega_H$, linear acceleration $a_H$, and gravitational acceleration $g_H$. These stimuli stimulate vestibular system receptors – angular velocity is detected by the SCC, and linear acceleration and gravity are detected by the OTO. After transformation to the SCC-fixed and OTO-fixed coordinate systems, respectively, these stimuli were used to create input vector u, which is recorded by vestibular system sensors (Fig. 7).

The outputs of the sensors (SCC and OTO) are the afferent neural signals $\alpha_{SCC}$ and $\alpha_{OTO}$, that represents sensed angular velocity, and gravito-inertial acceleration respectively. These signals creates the output vector y of the vestibular system sensor model (Fig. 7). The model of each of the sensors (SCC and OTO) can be expressed by the following two equations:

$$\dot{\mathbf{x}} = \mathbf{A} \cdot \mathbf{x} + \mathbf{B} \cdot \mathbf{u} \quad (18)$$

$$\mathbf{y} = \mathbf{C} \cdot \mathbf{x} + \mathbf{D} \cdot \mathbf{u} \quad (19)$$

where A and B are matrices for the state equation and C and D are matrices for the output equation. The state variables vector x, input signals vector u, and the output signals vector y are summarized in Tab. 5.

The mathematical model of the vestibular system, which allows us to determine the estimated response vector y for the SCC and the OTO sensors, is built based upon the knowledge of these functioning sensors. This description is supplemented with kinematic compounds and other relations between the calculated parameters. Finally, 27 variables are considered in the model as shown in Tab. 5. They are composed of the input vector u (6 variables), the state vector x (15 variables), and the output vector y (6 variables). The expressions for these vectors are specified below.

Components of input vector u are described in the following physical quantities:

– angular velocity vector in $Nx_{SCC}\,y_{SCC}\,z_{SCC}$ system

$$\Omega_{SCC} = L_{SCC/H} \cdot \Omega_H \quad (20)$$

– GIA vector in $Nx_{OTO}\,y_{OTO}\,z_{OTO}$ system

$$f_{OTO} = L_{OTO/H} \cdot f_H \quad (21)$$

for which $f_H$ acceleration in $Hx_H\,y_H\,z_H$ system is equal to (1), and

$$\mathbf{g}_H = \mathbf{L}_{H/E} \cdot [0\ 0\ g]^T \quad (22)$$

Tab. 5. Input, state, and output vectors in the model for the physical world.

| | Physical meaning | Equation |
|---|---|---|
| **Components of stimuli vector** | | |
| $\Omega_H=[p_H\ q_H\ r_H]^T$ | angular velocity vector in the head-fixed reference frame | |
| $a_H=[a_{XH}\ a_{YH}\ a_{ZH}]^T$ | linear acceleration vector in the head-fixed reference frame | |
| $g_H=[g_{XH}\ g_{YH}\ g_{ZH}]^T$ | gravity vector in the head-fixed reference frame | (22) |
| **Components of the input vector u** | | |
| $\Omega_{SCC}=[p_{SCC}\ q_{SCC}\ r_{SCC}]^T$ | angular velocity vector in the SCC-fixed reference frame | (20) |
| $f_{OTO}=[f_{xOTO}\ f_{yOTO}\ f_{zOTO}]^T$ | GIA vector in the OTO-fixed reference frame | (21) |
| **Components of the state vector x** | | |
| $[x_1, x_2, x_3, \ldots, x_{15}]^T$ | 15-element, variable vector for the state sensors vector | (18) |
| **Components of output vector y** | | |
| $\mathbf{y} = \begin{bmatrix}\tilde{\boldsymbol{\alpha}}_{SCC}\\ \tilde{\boldsymbol{\alpha}}_{OTO}\end{bmatrix}$ | $\tilde{\boldsymbol{\alpha}}_{SCC} = [\tilde{p}_{SCC}\ \tilde{q}_{SCC}\ \tilde{r}_{SCC}]^T$ angular velocity vector estimated using the SCC model | (19) |
| | $\tilde{\boldsymbol{\alpha}}_{OTO} = [\tilde{\alpha}_{x_{OTO}}\ \tilde{\alpha}_{y_{OTO}}\ \tilde{\alpha}_{z_{OTO}}]^T$ GIA vector estimated using the OTO model | (19) |

The matrix $L_{H/E}$ (15), which occurs in equation (22), was created based on the angles:

$$[\phi_H, \theta_H, \psi_H]^T = \int \mathbf{S}(\phi_H, \theta_H, \psi_H) \cdot \boldsymbol{\Omega}_H dt \tag{23}$$

where $S(\varphi_H,\theta_H,\psi_H)$ is the transformation matrix that converts the angular velocity vector from the $Hx_H\ y_H\ z_H$ system to the $Hx_E\ y_E\ z_E$ system. The elements of this matrix are as follows:

$$\mathbf{S}(\phi_H, \theta_H, \psi_H) == \begin{bmatrix} 1 & \sin\phi_H \cdot \tan\theta_G & \cos\phi_H \cdot \tan\theta_H \\ 0 & \cos\phi_H & -\sin\phi_H \\ 0 & \dfrac{\sin\phi_H}{\cos\theta_H} & \dfrac{\cos\phi_H}{\cos\theta_H} \end{bmatrix} \tag{24}$$

Decomposition of the transfer function (6) and (13) was performed to reveal the observability canonical form. In this way, variable state vector x was created. The general dynamic equations (18) and (19) have the following variables:

- the input vector

$$\mathbf{u} = [p_{SCC}\ q_{SCC}\ r_{SCC}\ f_{x_{OTO}}\ f_{y_{OTO}}\ f_{z_{OTO}}]^T$$

- matrices for the state equations:

$$\mathbf{A} = \begin{bmatrix} \mathbf{A}_\Omega & 0 \\ 0 & \mathbf{A}_f \end{bmatrix}, \quad \mathbf{B} = \begin{bmatrix} \mathbf{B}_\Omega & 0 \\ 0 & \mathbf{B}_f \end{bmatrix} \tag{25}$$

where

$$\mathbf{A}_\Omega = \begin{bmatrix} (z_1)_{p_{SCC}} & 1 & 0 & 0 & 0 & 0 & 0 & 0 & 0 \\ (z_2)_{p_{SCC}} & 0 & 1 & 0 & 0 & 0 & 0 & 0 & 0 \\ (z_3)_{p_{SCC}} & 0 & 0 & 0 & 0 & 0 & 0 & 0 & 0 \\ 0 & 0 & 0 & (z_1)_{q_{SCC}} & 1 & 0 & 0 & 0 & 0 \\ 0 & 0 & 0 & (z_2)_{q_{SCC}} & 0 & 1 & 0 & 0 & 0 \\ 0 & 0 & 0 & (z_3)_{q_{SCC}} & 0 & 0 & 0 & 0 & 0 \\ 0 & 0 & 0 & 0 & 0 & 0 & (z_1)_{r_{SCC}} & 1 & 0 \\ 0 & 0 & 0 & 0 & 0 & 0 & (z_2)_{r_{SCC}} & 0 & 1 \\ 0 & 0 & 0 & 0 & 0 & 0 & (z_3)_{r_{SCC}} & 0 & 0 \end{bmatrix}$$

$$\mathbf{A}_f = \begin{bmatrix} w_1 & 1 & 0 & 0 & 0 & 0 \\ w_2 & 0 & 0 & 0 & 0 & 0 \\ 0 & 0 & w_1 & 1 & 0 & 0 \\ 0 & 0 & w_2 & 0 & 0 & 0 \\ 0 & 0 & 0 & 0 & w_1 & 1 \\ 0 & 0 & 0 & 0 & w_2 & 0 \end{bmatrix} \tag{26}$$

for

$$(z_1)_{i_{SCC}} = -\frac{(\tau_1)_{i_{SCC}} + \tau_2}{(\tau_1)_{i_{SCC}}\tau_2} \qquad w_1 = -\frac{\tau_{1OTO} + \tau_{2OTO}}{\tau_{1OTO}\tau_{2OTO}}$$
$$(z_2)_{i_{SCC}} = -\frac{(\tau_1)_{i_{SCC}} + \tau_2 + \tau_A}{(\tau_1)_{i_{SCC}}\tau_2\tau_A} \qquad w_2 = -\frac{1}{\tau_{1OTO}\tau_{2OTO}}$$
$$(z_3)_{i_{SCC}} = -\frac{1}{(\tau_1)_{i_{SCC}}\tau_2\tau_A} \tag{27}$$

$(\ )i_{SCC}$ means the value of the i-th component with angular velocity (i=p,q,r) in the $Nx_{SCC}\ y_{SCC}\ z_{SCC}$ system.

$$\mathbf{B}_\Omega = \begin{bmatrix} \tau_L & 1 & 0 & 0 & 0 & 0 & 0 & 0 & 0 \\ 0 & 0 & 0 & \tau_L & 1 & 0 & 0 & 0 & 0 \\ 0 & 0 & 0 & 0 & 0 & 0 & \tau_L & 1 & 0 \end{bmatrix}^T$$

$$\mathbf{B}_f = \begin{bmatrix} w_3 & 0 & 0 \\ w_4 & 0 & 0 \\ 0 & w_3 & 0 \\ 0 & w_4 & 0 \\ 0 & 0 & w_3 \\ 0 & 0 & w_4 \end{bmatrix} \tag{28}$$

where

$$w_3 = \frac{K_{OTO} \cdot \tau_{LOTO}}{\tau_{1OTO} \cdot \tau_{2OTO}}, \qquad w_4 = \frac{K_{OTO}}{\tau_{1OTO} \cdot \tau_{2OTO}}$$

– matrices for the output equations:

$$\mathbf{C} = \begin{bmatrix} \mathbf{C}_\Omega & 0 \\ 0 & \mathbf{C}_f \end{bmatrix}, \ \mathbf{D} = \begin{bmatrix} \mathbf{D}_\Omega & 0 \\ 0 & \mathbf{D}_f \end{bmatrix} \tag{29}$$

where

$$\mathbf{C}_\Omega = \begin{bmatrix} 1 & 0 & 0 & 0 & 0 & 0 & 0 & 0 & 0 \\ 0 & 0 & 0 & 1 & 0 & 0 & 0 & 0 & 0 \\ 0 & 0 & 0 & 0 & 0 & 0 & 1 & 0 & 0 \end{bmatrix}$$

$$\mathbf{C}_f = \begin{bmatrix} 1 & 0 & 0 & 0 & 0 & 0 \\ 0 & 0 & 1 & 0 & 0 & 0 \\ 0 & 0 & 0 & 0 & 1 & 0 \end{bmatrix} \tag{30}$$

and $D_\Omega=0$ $D_f=0$

## Simulation of the pilot's motion sensation

To achieve the purpose of our work, the mathematical model of human vestibular receptors, as developed in the previous section, was used to perform simulations of the pilot's motion sensation during a 20-second real flight in an F-16 aircraft. Data from this flight was recorded in the Enhanced Crash Survivable Memory Unit (ECSMU) and was described in detail in the paper [41]. The model of human vestibular receptors was implemented in MATLAB-Simulink 2010a (The MathWorks, US) software suite. The Simulink model was configured with a variable time-step Runge-Kutta differential equation solver.

In the numerical calculations, the components of the angular velocity, linear acceleration and gravity are in respect to three reference frames: the pilot's head-fixed, SCC-fixed, and OTO-fixed reference frames. The linear acceleration includes the tangential and centrifugal accelerations occurring as a result of the aircraft's rotation and the pilot's head offsetting from the point of rotation (the aircraft's center of gravity). The components of angular velocity and linear acceleration acting on the pilot's head during the flight were calculated using the transformations described in the paper [41].

The anatomical arrangement of the SCCs (Tab. 4) and the OTO, with a 50-mm displacement of the vestibular system from the center of the head (Fig. 5), were included in the developed model. The model employs the utricular and saccular planes, which are assumed to pitched up relative to the horizontal plane of the head by an angle of $\theta_{OTO}$=30° (17).

Implementation of the vestibular system into the anatomy model (location and orientation of the SCCs and OTO receptors) leads to the use of the appropriate transformations of processed signals (vectors of the angular velocity and GIA). For this purpose, two matrices $L_{SCC/H}$ (16) and $L_{OTO/H}$ (17) were used to transform these signals from the head-fixed coordinate system to the SCC-fixed and the OTO-fixed reference frames respectively. It has been assumed that processing of the GIA vector (1) in the OTO model is carried out in the OTO-fixed reference frame. In the case of the estimated angular velocity, a similar assumption was used. The calculations for the $\Omega_{SCC}$ vector in the SCC-fixed reference frame were performed.

## Initial condition

In the calculations, the following initial conditions were assumed. The gravitational acceleration regularly experienced on Earth, and angles of attitude $\varphi_H$=-32.8°, $\theta_H$=-11° and $\psi_H$=56°. Additionally, it was assumed that the pilot keeps his head in the natural upright position, and during the flight, the pilot's head does not change its angular and linear positions with respect to the aircraft's center of gravity (CG). It was also assumed that, during the flight, the aircraft's CG does not change in position, e.g., as a result of fuel consumption. The analyzed, 20-second flight includes a right turn with a maximum, 5g positive acceleration and the barrel-roll maneuver. During the barrel roll, the pilot maintained an inverted flight for a few seconds.

## Simulation results and discussion

The simulation results for the components of the angular velocity vector and the gravito-inertial acceleration (GIA) vector are illustrated in Figs. 8 and 9, respectively. The components of the physical stimuli acting upon the pilot's head in flight are represented by red line, while components "sensed" by the pilot were represented by green (sensed in the SCC-fixed reference system) and blue (sensed in the head-fixed reference system) lines. Positive values are rightward motions from the pilot's perspective, while negative values represent leftward motions.

Because the characteristics for the human sensation of motion have been particularly popular in the literature [8,13,32,34,46,67,79,81], we will not go into these details. We limit this paper mainly to the issue of considering the explanation of the differences in the self-motion sensation estimated in the head- vs. SCC-fixed reference frame. It should be emphasized that the motion stimuli (angular velocity and linear acceleration) that occur in the

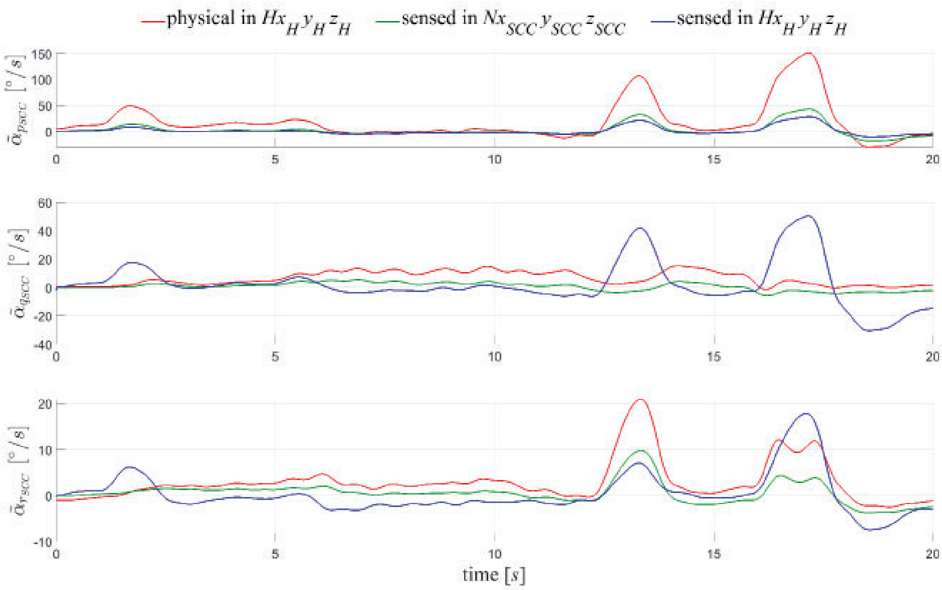


Fig. 8. The components of the physical and the pilot's sensed angular velocity vector in the head- and SCC-fixed reference frames.

flight environment often exhibit imperfections in the receptors of the vestibular system. These imperfections are mainly related to the receptors' inability to detect signals with values below their physiological detection thresholds ($TH_{SCC}$ and $TH_{OTO}$ in Tab. 2 & Tab. 3, respectively).

The pilot's sensation of the angular velocity (Fig. 8) indicates that each component computed in the SCC-fixed reference frame (green line) was different compared to their corresponding components computed in the head-fixed reference frame (blue line). These changes occur when physical velocity (red line) changes occur. The largest changes in the value of the physical angular velocity (red line) occurred for the roll angular velocity (p) that describes the rotation of the aircraft with respect to the longitudinal axis.

The differences in the pilot's sensed angular velocity, as seen in Fig. 8 (green vs. blue line), result from the transformation $L_{SCC/H}$ (16) of the physical velocity components (red line) to the SCC-fixed reference frame. This is noticeable at 2, 13, and 17 sec of flight, where the roll rate component p of the aircraft's angular-velocity vector occurs. This transformation of the roll rate results in additional angular velocities (q, r) acting in the pitch and yaw planes of the SCCs. For the analyzed case, the most visible differences in the sensed angular velocities occur at the pitch rate component $q_{SCC}$. The pitch angular velocity $q_{SCC}$ sensed by the pilot is downward if the roll angular velocity (red line) is to the right. Otherwise, the pitch velocity is upward. However, it is difficult to find a confirmation of this pitching sensation in the literature. Most of the studies [9,37,38,46,48,61] and [11,12,77,33,70–76] concerned with the static roll tilt perception in the hyper-gravity-induced environment, e.g., the roll tilt of the whole body or only the head. In these studies, the hyper-gravity environment was created using a centrifuge. The roll tilts utilized causes a cross-coupled illusion during the planetary spin of the centrifuge necessary to create hyper-gravity. Clark et al. [11] found that this cross-coupled stimulus provoked an illusory pitching sensation. At the same time, the authors point out that this cross-coupled illusion would not occur in a "pure" hyper-gravity environment, such as that experienced in a high-performance aircraft performing a constant bank angle turn with a very large radius. Thus, the only way to verify that the cross-coupled stimulus issue did not impact the sensation of the pitch velocity is to conduct the experiments in a non-spinning environment.

Components of the gravito-inertial acceleration sensed by the pilot are shown in (Fig. 9). All of these components (green and blue line) have a similar shape, but for the longitudinal $\alpha_{xOTO}$ component, the changes are much different.

The differences in the pilot's sensed gravito-inertial acceleration $\alpha_{OTO}$ (Fig. 9), green and blue line, especially for the longitudinal acceleration component $\alpha_{xOTO}$ results from the performed transformation $L_{OTO/H}$ (17) of the physical acceleration (red line). In the calculation, the utricular plane's tilt

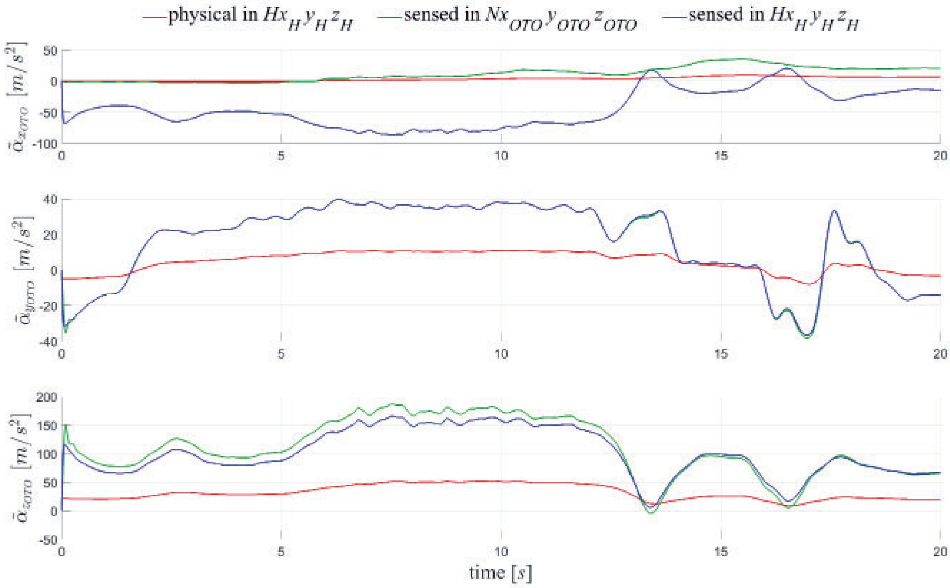


Fig. 9. The components of the physical and the pilot's sensed gravito-inertial acceleration vector.

angle $\theta_{OTO}$=30° relative to the horizontal plane of the head-fixed reference frame was used (Fig. 5). Thus, when the vertical components of the acceleration $a_z$ and gravity $g_z$ relative to the head-fixed reference frame, are converted to the OTO-fixed reference frame, the results is an additional longitudinal acceleration $a_x$ and $g_x$, respectively.

The apparent change in sensed GIA at 13 and 17 sec of flight (Fig. 9) may be attributed to the aircraft's roll angular velocity (Fig. 8). According to Ish-Shalom [36], at maximum head rotation speeds of 1500 °/sec, the centripetal forces acting on the vestibular system can be up to 4 g. It comes from the fact that each vestibular system in the inner ear is not located at the center of the head. In this complex motion (the sixth degree of freedom for aircraft motion and the pilot's head), the inertial linear acceleration $a_N$ (1) acting on the vestibular system is the sum of the following acceleration components [3]:

$$a_N=a_{AC}+a_\epsilon+a_\Omega+a_{W\epsilon}+a_{W\Omega}+a_{Cor} \quad (31$$

where

$a_{AC}=\partial V_{AC}/\partial t+\Omega_{AC}\times V_{AC}$ is an absolute acceleration for the aircraft's CG ($V_{AC}$ and $\Omega_{AC}$ are the aircraft's linear and angular velocities, respectively),

$a_\epsilon=\epsilon_{AC}\times(l_H+l_h)$ is the tangential acceleration ($\epsilon_{AC}$ – vector for the aircraft's angular acceleration, – vector for the distance of the head from the aircraft's CG, $l_h$– vector for the distance of the vestibular system from the center of the head (origin of the head-fixed coordinate system, Fig. 5),

$a_\Omega=\Omega_{AC}\times[\Omega_{AC}\times(l_H+l_h)]$ is a centrifugal acceleration,

$a_{W\epsilon}=\epsilon_{H/AC}\times l_h$ is the relative tangential acceleration,

$a_{W\Omega}=\Omega_{H/AC}\times(\Omega_{H/AC}\times l_h)$ is the relative centrifugal acceleration,

$a_{Cor}=2\Omega_{AC}\times(\Omega_{H/AC}\times l_h)$ is the Coriolis acceleration.

In the considered cases of motion (a simplified assumption is that the pilot does not rotate his head $\Omega_{H/AC}$=0), the following acceleration components do not occur: $a_{W\Omega}$, $a_{Cor}$ and $a_{W\epsilon}$. The tangential $a_\epsilon$ and centrifugal $a_\Omega$ accelerations are due to the rotation of the aircraft relative to the CG, the presence of the head offset $l_H$, and to the vestibular system offset $l_h$. The results shown in Fig. 9 were obtained for the head offset of $l_H$=[4.5 0 0.5]$^T$ described in the body-fixed coordinate system for the aircraft [6,41], and for the vestibular system offset of $l_h$=[0 0.05 0]$^T$ as described in the head-fixed reference frame. In the analyzed flight phase, for the largest angular velocity component p=150 °/s (about 17 sec of the flight), the magnitude of the accelerations generated by these shifts ($l_H+l_h$) are equal: $a_\epsilon\approx$-4.76 m/s$^2$ and $a_\Omega\approx$5.82 m/s$^2$. Considering only the head offset $l_H$, these accelerations have the same magnitudes. So, we can see that accelerations generated by the vestibular system offset $l_h$ are not significant, so they should not effect a pilot's sensed gravito-inertial acceleration $\alpha_{OTO}$ (Fig. 9). This assumption excludes the sensing of rotation by the otolith organs due to centripetal and tangential accelerations. Considering only the case of the head offset $l_H$ relative to the aircraft's CG, the tangential $a_\epsilon$ and centrifugal $a_\Omega$ accelerations will be included in the vertical $a_z$ and lateral ay components of the physical acceleration (31). This is particularly evident at 13 and 17 sec of the flight, where these components change significantly (Fig. 9). For this reason, it is important to include the aircraft's rotation and the head offset $l_H$ in determining the tangential $a_\epsilon$ and centrifugal $a_\Omega$ accelerations that effect a pilot's head. In summary, we can say that the estimated sensation of human linear acceleration in the SCC-fixed reference frame is differ from the sensation of acceleration calculated in the head-fixed reference frame. This particularly applies to the longitudinal acceleration component when the vertical component achieves high values.

Finally, it is important to note the consequence of the principle of equivalence, which states that no gravireceptors can differ between gravity and inertia. As a result, angular changes in the roll and yaw positions, which occur during certain common flight maneuvers, cannot be detected using the otolith organs. It can be observed when the pilot performs a coordinated turn (red line in Fig. 9, a right turn with maximum positive acceleration of 5g, from 5 to 12 sec). He then experiences an increasing GIA vector acting in parallel with his head and his body's vertical axis. Therefore, the signal from the otolith organs is that the pilot remains upright (sensed by the pilot). However, to the vertical SCCs, the roll angular displacement (i.e., the change in roll position) is a stimulus similar to that occurring when tilting one's head towards one's shoulder [81].

## Study limitations

The study did not include the threshold stimulus (angular velocity < $TH_{SCC}$) with the performance of the flight maneuvers, which was most important for flight safety (i.e., the pilot's loss of orientation). Additionally, the model of vestibular system receptors has been validated for experimental conditions other than those used in this study. In the validation procedure, subjects were passively accelerated (i.e., they did not control the motions they experienced), while during flight, the pilot was actively accelerated (i.e., the pilot controlled the motions that he experienced). The responses of the vestibular nuclei neurons were markedly suppressed for being active when compared to passive motion restricted to stimulating a single modality (e.g., canals [58,59]; otoliths [7]. Carriot et al. [8] have checked how information about rotational and translational components for self-motion are integrated by vestibular pathways during active and/or passive motion. The authors found that, in response to active stimulation, neuronal modulation was significantly attenuated (<70%) relative to passive stimulation for rotations and translations, and were even more profoundly attenuated for combined motion due to sub-additive input integration. For this reason, this study should be repeated after re-validation of the model using data for active motion.

Future studies should also include the effects of hypo-gravity on the estimation of self-motion perception (i.e., <1 g sometimes when flying in a fast jet aircraft). Moreover, it is not clear whether similar variations in the estimated pilot's sensation of motion and orientation would occur if different stimuli profiles (i.e., a complex vestibular stimuli) or different attitude representation were used. Thus, future studies should also consider these issues.

## CONCLUSIONS

The paper presents the procedure of a physical and mathematical modeling of the human sensation of self-motion based upon the vestibular system. The aim of this study was also to test whether an increased complexity of the model, specifically regarding the anatomy (position and orientation) of vestibular receptors (semicircular canals and otolith organs), could significantly influence the estimation of human self-motion sensation. From the conducted simulations for the motion of the pilot using two reference systems – head-fixed and vestibular-fixed (SCC & OTO) reference frames – we found that:

- the estimated sensation of human angular velocity differs, this particularly applies to the pitch angular velocity when the roll velocity is present;
- the sensed gravito-inertial acceleration differs, particularly with the longitudinal acceleration when the vertical acceleration achieves high values;

– although this has not been verified, it can be assumed that the non-rectangular, SCC-fixed coordinate system does not need to be used to correctly describe the perception of angular velocity. It is therefore possible to simplify this coordinate system to a rectangular one.

In conclusion, these findings indicate that the inclusion of SCC and OTO orientation in models of these receptors affects the estimated motion sensation. It is important to note that the orientation of the receptors has no effect on the model predictions as long as an identical geometrical orientation is included in the internal model of these receptors [47]. However, to confirm these findings and evaluate their practical implications in areas such as motion perception, further research and verification are necessary.

In studies on flight safety, it is crucial to consider the rotation of the aircraft and the head offset $l_H$ when determining the tangential $a_\epsilon$ and centrifugal $a_\Omega$ accelerations that affect a pilot's head. Furthermore, research has shown that the vestibular system offset $l_h$ (distance from the centre of the head) does not affect the pilot's sensation of linear acceleration and can therefore be excluded from the calculations.

Despite numerous simplifications and limitations (i.e., only one model, located at the center of the head, is used to represent both vestibular organs), the presented model can be a useful tool for scientific research work pertaining to the improvement of existing and newly developing simulators equipped with the motion platform. Moreover, it is possible to apply this model to other areas; for example, in medical diagnoses to simulate vestibular system dysfunction [57,66], or for assessing the pathology of the human equilibrium apparatus and the development of prosthetic rehabilitation for this organ.

## AUTHORS' DECLARATION:

**Study Design:** Rafał Lewkowicz, Grzegorz Kowaleczko. **Data Collection:** Rafał Lewkowicz, Grzegorz Kowaleczko. **Manuscript Preparation:** Rafał Lewkowicz, Grzegorz Kowaleczko. The Authors declare that there is no conflict of interest.

## REFERENCES

1. Blausen.com staff. Medical gallery of Blausen Medical 2014. WikiJournal Med. 2014; 1(2).
2. Bradshaw AP, Curthoys IS, Todd MJ, Magnussen JS, Taubman DS, Aw ST, et al. A mathematical model of human semicircular canal geometry: A new basis for interpreting vestibular physiology. J Assoc Res Otolaryngol. 2010; 11(2):145–59.
3. Brizard A. Motion in a non-inertial frame. In: An Introduction to Lagrangian Mechanics. 2nd ed. Colchester, VT: Saint Michael's College; 2015. p. 161–79.
4. Bronzino JD. Biomedical Engineering Handbook. 3rd ed. CRC Press Taylor & Francis Group; 2006. 1569 p.
5. van Buskirk WC, Watts RG, Liu YK. The fluid mechanics of the semicircural canals. J Fluid Mech. 1976; 78(1):87–98.
6. Cai G, Chen BM, Lee TH. Coordinate Systems and Transformations. In: Unmanned Rotorcraft Systems. London, UK: Springer--Verlag; 2011. p. 23–35.
7. Carriot J, Brooks JX, Cullen KE. Multimodal Integration of Self-Motion Cues in the Vestibular System: Active versus Passive Translations. J Neurosci. 2013; 33(50):19555–66.
8. Carriot J, Jamali M, Brooks JX, Cullen KE. Integration of canal and otolith inputs by central vestibular neurons is subadditive for both active and passive self-motion: implication for perception. J Neurosci. 2015; 35(8):3555–65.
9. Chelette TL, Martin EJ, Albery WB. The effect of head tilt on perception of self-orientation while in a greater than one G environment. J Vestib Res. IOS Press; 1995; 5(1):1–17.
10. Cheng Z, Gu Y. Vestibular system and self-motion. Front Cell Neurosci. 2018; 12:1–9.
11. Clark TK, Newman MC, Oman CM, Merfeld DM, Young LR. Human perceptual overestimation of whole body roll tilt in hypergravity. J Neurophysiol. 2015; 113(7):2062–77.
12. Clark TK, Newman MC, Oman CM, Merfeld DM, Young LR. Modeling human perception of orientation in altered gravity. Front Syst Neurosci. 2015; 9(68):1–13.
13. Clément GR, Moore ST, Raphan T, Cohen B. Perception of tilt (somatogravic illusion) in response to sustained linear acceleration during space flight. Exp Brain Res. 2001; 138(4):410–8.

14. Cohen MM, Crosbie RJ, Blackburn LH. Disorienting effects of aircraft catapult launchings. Aerosp Med. United States; 1973; 44(1):37–9.

15. Constantinescu VD. Revealing the distinction between perception and cognition through intra-individual variability of visual evoked responses. Int J Biomed Comput. Elsevier; 1996; 40(3):169–78.

16. Corvera J, Hallpike CS, Schuster EHJ. A new method for the anatomical reconstruction of the human macular planes. Acta Otolaryngol. Taylor & Francis; 1958; 49(1):4–16.

17. Curthoys IS, Oman CM. Dimensions of the Horizontal Semicircular Duct, Ampulla and Utricle in the Human. Acta Otolaryngol. 1987; 103(5):254–61.

18. Curthoys IS, Betts GA, Burgess AM, MacDougall HG, Cartwright AD, Halmagyi GM. The planes of the utricular and saccular maculae of the guinea pig. Ann N Y Acad Sci. Wiley Online Library; 1999; 871(1):27–34.

19. Curthoys IS, Blanks RH, Markham CH. Semicircular canal functional anatomy in cat, guinea pig and man. Acta Otolaryngol. England; 1977; 83(3–4):258–65.

20. van Egmond AAJ, Groen JJ, Jongkees LBW. The mechanics of the semicircular canal. J Physiol. 1949; 110(1–2):1–17.

21. Fernandez C, Goldberg JM. Physiology of Peripheral Neurons Innervating Otolith Organs of the Squirrel Monkey. I. Response to static tilts and to long-duration centrifugal force. J Neurophysiol. 1976; 39(5):970–84.

22. Fernandez C, Goldberg JM. Physiology of peripheral neurons innervating semicircular canals of the squirrel monkey. II. Response to sinusoidal stimulation and dynamics of peripheral vestibular system. J Neurophysiol. 1971; 34(4):661–75.

23. Fucke L, Groen E, Goman M, Abramov N, Wentink M, Nooij S, et al. Final results of the supra project: Improved Simulation of Upset Recovery. 28th Congr Int Counc Aeronaut Sci 2012, ICAS 2012. 2012; 6:4607–16.

24. Gillingham KK, Previc FH. Spatial orientation in flight. Report No. AL-TR-1993-0022. San Antonio, TX; 1993.

25. Grant JW, Best WA. Otolith-Organ Mechanics: Lumped Parameter Model and Dynamic Response. Aviat Space Environ Med. 1987; 58(10):970–6.

26. Grant JW, Cotton JR. A model for otolith dynamic response with a viscoelastic gel layer. J Vestib Res. 1990; 1(2):139–51.

27. Groen E, Field JN, Ledegang W, Nooij S, Zaichik L, Fucke L, et al. SUPRA - Enhanced Upset Recovery Simulation. In: AIAA Modelling and Simulation Technologies Conference. Minneapolis, MN; 2012.

28. Groen JJ, Lowenstein O, Vendrik AJH. The mechanical analysis of the responses from the end-organs of the horizontal semicircular canal in the isolated elasmobranch labyrinth. J Physiol. 1952; 117(3):329–46.

29. Hain TC, Helminski JO. Anatomy and Physiology of the Normal Vestibular System. In: Herdman SJ, Clendaniel RA, editors. Vestibular Rehabilitation. 4th ed. Philadelphia, PA: F. A. Davis Company; 2014. p. 2–18.

30. Hao C, Fan X, Dong C, Qiao L, Li X, Li X, et al. A Classification Method for Unrecognized Spatial Disorientation Based on Perceptual Process. IEEE Access. 2020; 8:140654–60.

31. Hashimoto S, Naganuma H, Tokumasu K, Itoh A, Okamoto M. Three-dimensional reconstruction of the human semicircular canals and measurement of each membranous canal plane defined by Reid's stereotactic coordinates. Ann Otol Rhinol Laryngol. SAGE Publications Sage CA: Los Angeles, CA; 2005; 114(12):934–8.

32. Holly JE, Davis SM, Sullivan KE. Differences between perception and eye movements during complex motions. J Vestib Res. 2011; 21(4):193–208.

33. Holly JE, Vrublevskis A, Carlson LE. Whole-motion model of perception during forward- and backward-facing centrifuge runs. J Vestib Res. 2008; 18(4):171–86.

34. Hosman RJAW. Pilot's Perception and Control of Aircraft Motions. PhD dissertation. Delft University of Technology; 1996.

35. Ifediba MA, Rajguru SM, Hullar TE, Rabbitt RD. The Role of 3-canals biomechanics in angular motion transduction by the human vestibular labyrinth. Ann Biomed Eng. 2007; 35(7):1247–63.

36. Ish-Shalom J. The design of optimal control motion for flight simulators. PhD dissertation. Massachusetts Institute of Technology; 1982.

37. Jarchow T, Wirz M, Haslwanter T, Dietz V, Straumann D. Perceived Horizontal Body Position in Healthy and Paraplegic Subjects: Effect of Centrifugation. J Neurophysiol. 2003; 90(5):2973–7.

38. Jia H, Yu L, Bi H, Wang K, Liu Z, Xie S. Perception of the cabin attitude changes in hypergravity. Aviat Space Environ Med. 2002; 73(3):191–3.

39. Lewkowicz R. Models of the human vestibular system receptors and physiological phenomena accompanying their stimulation [Modele receptorów narządu przedsionkowego człowieka oraz zjawisk fizjologicznych towarzyszących ich pobudzeniom]. (Polish). Model inżynierskie. 2016; 27(58):83–104. (in Polish)

40. Lewkowicz R. An optimal motion cueing algorithm with LQR for inducing the leans illusion in a flight simulator equipped with the Stewart-Gough platform [Algorytm optymalnego bodźcowania ruchowego z LQR do generowania złudzenia przechylenia

w symulatorze lotu z platformą Stewarta-Gougha]. In: Sybilski K, Lichota P, editors. Mechanika w Lotnictwie ML-XX. Kazimierz Dolny: Instytut Techniczny Wojsk Lotniczych; 2022. p. 251–76. (in Polish)

41. Lewkowicz R. The use of a dynamic flight simulator for aviation mishap investigation [Dochodzenie w sprawie wypadku lotniczego z zastosowaniem dynamicznego symulatora lotu]. In: Sibilski K, Lichota P, editors. Mechanika w Lotnictwie ML-XIX. Warszawa: Instytut Techniczny Wojsk Lotniczych; 2020. p. 131–51. (in Polish)
42. Lewkowicz R, Kowaleczko G. Modeling of the pilot's vestibular system for the evaluation of the control algorithm of the flight simulator motion system [Modelowanie układu przedsionkowego pilota na potrzeby oceny algorytmu sterowania układem ruchu symulatora lotu]. In: Sibilski K, editor. Mechanika w Lotnictwie ML-XVII. 1st ed. Kazimierz Dolny: Polskie Towarzystwo Mechaniki Teoretycznej i Stosowanej; 2016. p. 247–62. (in Polish)
43. Lewkowicz R, Kowaleczko G. Kinematic issues of a spatial disorientation simulator. Mech Mach Theory. 2019; 138:169–81.
44. Mayne R. The audiogyral illusion and the mechanism of spatial representation. Bull Math Biophisics. 1952; 14(1):27–34.
45. Meiry JL. The vestibular system and human dynamic space orientation. PhD dissertation. Massachusetts Institute of Technology; 1965.
46. Merfeld DM, Park S, Gianna-Poulin C, Black FO, Wood S. Vestibular perception and action employ qualitatively different mechanisms. II. VOR and perceptual responses during combined Tilt & Translation. J Neurophysiol. 2005; 94(1):199–205.
47. Merfeld DM, Zupan LH. Neural processing of gravitoinertial cues in humans. III. Modeling tilt and translation responses. J Neurophysiol. 2002; 87(2):819–833.
48. Merfeld DM, Zupan LH, Gifford CA. Neural processing of gravito-inertial cues in humans. II. Influence of the semicircular canals during eccentric rotation. J Neurophysiol. 2001; 85(4):1648–60.
49. Mumaw, R J, Groen EL, Fucke L, Anderson R, Bos JE, Houben M. A new tool for analyzing the potential influence of vestibular illusions. In: ISASI Forum, Journal of the International Society of Air Safety Investigators 49. Augsburg, Germany; 2016. p. 6–12.
50. Newman MC. A multisensory observer model for human spatial orientation perception. MSc thesis. Massachusetts Institute of Technology: Cambridge; 2009.
51. Newman MC, Lawson BD, McGrath BJ, Rupert AH. Perceptual modeling as a tool to prevent aircraft upset associated with spatial disorientation. In: Proceedings of the AIAA Guidance, Navigation, and Control Conference. National Harbor, MD; 2014. p. 1–12.
52. Obrist D. Fluidmechanics of semicircular canals - revisited. Zeitschrift für Angew Math und Phys. 2008; 59(3):475–97.
53. Obrist D, Hegemann S, Kronenberg D, Hauselmann O, Rosgen T. In vitro model of a semicircular canal: Design and validation of the model and its use for the study of canalithiasis. J Biomech. 2010; 43(6):1208–14.
54. Oman CM. Influence of adaptation on the human semicircular canals and the role of subjective angular velocity cues in spatial orientation. MSc. thesis. Massachusetts Institute of Technology; 1968.
55. Oman CM, Marcus EN, Curthoys IS. The influence of semicircular canal morphology on endolymph flow dynamics. An anatomically descriptive mathematical model. Acta Otolaryngol. 1987; 103(1–2):1–13.
56. Rabbitt RD, Damiano ER, Grant JW. Biomechanics of the Semicircular Canals and Otolith Organs. In: Highstein SM, Fay RR, Popper AN, editors. The vestibular system. New York, NY: Springer US; 2004. p. 153–201.
57. Rajguru SM, Rabbitt RD. Afferent responses during experimentally induced semicircular canalithiasis. J Neurophysiol. 2007; 97(3):2355–63.
58. Roy JE. Dissociating Self-Generated from Passively Applied Head Motion: Neural Mechanisms in the Vestibular Nuclei. J Neurosci. 2004; 24(9):2102–11.
59. Roy JE, Cullen KE. Selective processing of vestibular reafference during self-generated head motion. J Neurosci. 2001; 21(6):2131–42.
60. Della Santina CC, Potyagaylo V, Migliaccio AA, Minor LB, Carey JP. Orientation of human semicircular canals measured by three-dimensional multiplanar CT reconstruction. J Assoc Res Otolaryngol. 2005; 6(3):191–206.
61. Schöne H, Parker DE, Mortag HG. Subjective vertical as a function of body position and gravity magnitude. Naturwissenschaften. 1967; 54(11):288.
62. Selva P. Modeling of the vestibular system and nonlinear models for human spatial orientation perception. PhD dissertation. Université de Toulouse; 2009.
63. Silverthorn DU. Human Physiology: An Integrated Approach. 5th ed. Regulation. San Francisco, CA: Pearson Benjamin Cummings; 2007. 992 p.
64. Small RL, Keller JW, Wickens CD, Oman CM, Jones TD. Modeling and mitigating spatial disorientation in low G environments: year 3 report. NSBRI Project Number SA 01302. Cambridge, MA; 2010.
65. Soyka F. Modeling Self-Motion Perception based on the Vestibular System. In: 13th Conference of the Junior Neuroscientists

of Tübingen (NeNA 2012): Science and Education as Social Transforming Agents. 2012. p. 13.

66. Squires TM, Weidman MS, Hain TC, Stone HA. A mathematical model for top-shelf vertigo: The role of sedimenting otoconia in BPPV. J Biomech. 2004; 37:1137–46.

67. van Der Steen H. Self-motion perception. PhD dissertation. Delft University of Technology; 1998.

68. Steer RW. The Influence of Angular and Linear Acceleration and Thermal Stimulation on the Human Semicircular Canals. PhD dissertation. Massachusetts Institute of Technology; 1967.

69. Tong F. Primary visual cortex and visual awareness. Nat Rev Neurosci. England; 2003 Mar; 4(3):219–29.

70. Tribukait A, Bergsten E, Eiken O. Pitch-plane angular displacement perception during helicopter flight and gondola centrifugation. Aerosp Med Hum Perform. 2016; 87(10):852–61.

71. Tribukait A, Bergsten E, Eiken O. Vestibular stimulus and perceived roll tilt during coordinated turns in aircraft and gondola centrifuge. Aerosp Med Hum Perform. 2016; 87(5):454–463.

72. Tribukait A, Bergsten E, Eiken O. Variability in perceived tilt during a roll plane canal-otolith conflict in a gondola centrifuge. Aviat Space Environ Med. 2013; 84(11):1131–9.

73. Tribukait A, Eiken O. Semicircular canal influence on the visually perceived eye level during gondola centrifugation. Aviat Space Environ Med. 2006; 77(5):500–8.

74. Tribukait A, Eiken O. On the role of otoliths and semicircular canals in spatial orientation: Dynamics of the visually perceived eye level during gondola centrifugation. Percept Psychophys. 2005; 67(7):1242–51.

75. Tribukait A, Eiken O. Roll-tilt perception during gondola centrifugation: Influence of steady-state acceleration (G) level. Aviat Space Environ Med. 2006; 77(7):695–703.

76. Tribukait A, Eiken O. Flight experience and the perception of pitch angular displacements in a gondola centrifuge. Aviat Space Environ Med. 2012; 83(5):496–503.

77. Tribukait A, Eiken O. Semicircular canal contribution to the perception of roll tilt during gondola centrifugation. Aviat Space Environ Med. 2005; 76(10):940–6.

78. Vidaković J, Kvrgić V, Lazarevic MP, Stepanić P. Computed torque control for a spatial disorientation trainer. FACTA Univ Ser Mech Eng. 2020; :1–12.

79. Winkel KN. Multisensory perception of spatial orientation and self-motion. PhD dissertation. Utrecht University; 2013.

80. Young LR. Optimal estimator models for spatial orientation and vestibular nystagmus. Exp Brain Res. 2011; 210(3–4):465–76.

81. Young LR. Perception of the body in space: Mechanisms. In: Darian Smith I, editor. Handbook of Physiology: The nervous system III. 2nd ed. Oxford University Press Inc.; 1984. p. 301–44.

82. Young LR, Meiry JL. A revised dynamic otolith model. Aerosp Med. 1968; 39(6):606–8.

83. Zacharias GL. Motion cue models for pilot-vehicle analysis. Report No. AM4RL-TR-78-2. Wright Patterson Air Base, Ohio; 1978.

84. Zaichik L, Yashin Y, Desyatnik P, Arkhangelsky Y. Motion cueing fidelity in upset recovery simulation. In: AIAA Scitech 2019 Forum. Reston, Virginia: American Institute of Aeronautics and Astronautics; 2019.

**Cite this article as**: Lewkowicz R, Kowaleczko G. Anatomy-Based Modelling of the Human Vestibular Receptors for the Purpose of Motion Cueing in Dynamic Flight Simulators. Pol J Aviat Med Bioeng Psychol 2021; 27(3): 5-24. DOI: 10.13174/pjambp.30.08.2024.01.